

Thermodynamic properties of chemically disordered compounds via AI-driven estimation of partition function with the PULSE method

Baptiste Bernard^a, Luca Messina^a, Eiji Kawasaki^b, Emeric Bourasseau^a

^a*CEA DES IRESNE DEC Cadarache F-13108 Saint-Paul-Lez-Durance France*

^b*Universite Paris-Saclay CEA LIST F-91120 Palaiseau France*

Abstract

In this article, we present an improved version of the PULSE method (Partition function Unsupervised Learning Sampling and Evaluation) for estimating the thermodynamic properties of chemically disordered compounds. The aim is to reduce the computational cost of Monte Carlo approaches for this type of material and to demonstrate that this generative tool can estimate thermodynamic properties by sampling and estimating the partition function of the system. To validate this innovative approach, we use the 2D Ising model as a benchmark. We demonstrate that our method accurately reproduces average properties with high precision and efficiency compared to traditional Monte Carlo sampling methods. Our results highlight the efficiency and adaptability of the PULSE method, making it a valuable tool for studying materials for which conventional methods are too inefficient to compute properties affected by chemical disorder at low cost.

1. Introduction

Nuclear safety and reactor operation efficiency require an accurate characterisation of material properties. However, performing experiments in the nuclear domain is often challenging. Indeed, radioactivity and the extreme operating conditions for materials in a nuclear reactor are difficult to reproduce in order to obtain measurements of the desired properties in the desired conditions. Meticulous modelling of materials at different scales is thus required in order to gain a thorough understanding of the physical phenomena at work in these materials. That is why, to complement experiments and macro-scale simulations, atomic-scale calculations are common in this field, and have already given very satisfying results, especially when applied to standard fuels like uranium dioxide or to structural materials [1, 2]. Therefore, as the emergence of novel multi-component materials - e.g., high-entropy alloys (HEA) [3, 4] or (U,Pu)O₂ mixed-oxide (MOX) fuels - opens innovative applications in the nuclear industry [5, 6, 7, 8, 9], it poses at the same time significant challenges for their atomic-scale modeling. In particular, the accurate evaluation of their thermodynamic properties remains a key issue for their use in nuclear environments.

These materials challenge our current understanding of the physics behind high-dimension spaces, as they are characterized by a large space of possible atomic configurations due to chemical disorder. Chemical disorder refers to the exponential growth in the number of possible configurations

of atomic species on the crystal lattice owing to the random occupation of atomic sites. Therefore, although traditional methods exist for sampling and computing properties for these materials [1, 2], they have inherent flaws that make them ineffective in certain respects. For instance, the use of Special Quasirandom Structures (SQS) is a common approach to study high-entropy alloys [10, 11, 12], but lacks criteria for determining the representativeness of the generated configurations. Also, classic Monte Carlo methods, although capable of estimating target properties, are computationally inefficient as they require the generation of a large number of configurations before convergence, making them very costly. For instance, a Monte Carlo evaluation of thermodynamic properties in MOX fuels needed over 100 million configurations to converge [13].

Recently, the approach to this type of problem has been strongly impacted by the introduction of Machine Learning (ML) methods, which make possible to optimize overly complex calculations thanks to their generalization capabilities. This is especially true since the advent of deep learning [14] and neural networks applied to the study of physical systems. This type of approach has proven effective when modelling disordered physical systems [15], in particular by introducing innovative ways of addressing the atomic scale in a multiscale modelling framework [16] using unsupervised ML methods. In this context, we have introduced in a previous work PULSE [17] (Partition function Unsupervised Learning

Sampling and Evaluation for disordered compounds), a general ML tool that aims to estimate observable properties of an atomic-scale physical system formulated as partition functions. Inspired by an inverse variational autoencoder architecture (VAE) [18], this method uses generative sampling to find the smallest set of significant configurations of the system in order to compute its mean properties. However, this tool was designed to estimate local properties such as defect formation energies in the atomic lattice [17], and was therefore not suitable for obtaining thermodynamic properties, which are inherently global and thus need considering atomic systems of much larger sizes.

In this work, we improve the PULSE method to make it suitable for the estimation of general observable properties of multi-component systems, including thermodynamic properties. One of the main objectives is to minimise the number of configurations needed, thereby minimising the computational resources required to estimate a property. As a first application, we decide to test the advantages and limitations of this new approach on a model system governed by equations similar to those of the target materials. The well-known Ising system appears to be an ideal testing ground for our target approach. Indeed, this system has been extensively studied from a sampling perspective [19, 20] because it is analytically solvable in the 2D case without an external magnetic field [21] and because calculations on this system can be carried out at low cost. This allows us to benchmark the results of PULSE against exact solutions. Moreover, over the last ten years, a wide range of ML models have been trying to explore the properties of this system, ranging from supervised [22, 23] to unsupervised learning [24, 25, 26, 27, 28, 29, 30]. We thus use the Ising model as an analogue of a two-component chemically disordered system, and we probe its physical properties with PULSE.

After introducing the extended PULSE mathematical framework and the Ising counterpart, we conduct performance tests on our method for estimating magnetic susceptibility. We continue this testing phase by investigating scaling as we increase the size of the Ising systems under study. Finally, we compare our method with other Monte Carlo methods suited to the study of the Ising system.

Once the results are presented, we draw conclusions that will show us how to apply PULSE on the prediction of thermal properties for more complex multi-component systems, such as MOX and HEA for nuclear applications.

2. PULSE methodology

In this section, we introduce the main features of PULSE. The principle is to identify and generate the smallest set of significant configurations that provides an accurate estimate of the target property in the large configuration space of a chemically disordered compound. The tool learns the physics of the system through its partition function. Sampling seeks

the right balance between a configuration’s probability (i.e., with low energy) and its contribution to the target property, as there can be low-probability configurations where this property has a large value, and vice versa high-probability ones where the value of this property is small.

The PULSE method [17] is based on unsupervised VAE [31] ML models. However, VAEs considered here are used in an "inverse" version, in order to reproduce the hidden complex distribution (i.e., that of atomic configurations) by generating samples from a chosen and simple distribution. With respect to classic VAEs, the role of encoder and decoder is thus inverted.

PULSE training proceeds via an unsupervised loop with no prior dataset. In each iteration, PULSE samples configurations from a latent space. The model is trained in such a way that, for each iteration, configuration energies are computed with a dedicated method of choice (for instance, *ab initio* calculations, or interatomic potentials). The calculated energies are used to determine the error, which enables backpropagation to update the weights of the network and the latent space. This process is repeated until convergence and then the value of the loss provides an estimate of the target partition function.

The goal of the present study is to improve the PULSE method by generalizing the approach to any partition function defined with respect to an observable property of the system. In what follows, we introduce a general formulation that allows us to describe a generic thermodynamic observable property.

2.1. Formulation of the target property in the Pulse framework

Let O be an observable property of a given physical system whose possible discrete states x belong to the configuration space X . We define the partition function of this property at temperature T by $Z_O(T)$:

$$Z_O(T) = \sum_{x \in X} O(x) \exp\left(\frac{-E(x)}{k_B T}\right). \quad (1)$$

A way to define the thermodynamic average of the property among the possible configurations is :

$$\langle O(T) \rangle = \frac{Z_O(T)}{Z(T)}. \quad (2)$$

with $Z(T)$ being the canonical partition function of the physical system. Our objective is to calculate this average by estimating both partition functions independently using the PULSE algorithm.

To do so, we define $P_O(x)$ as the probability for the property to have the value $O(x)$ in the configuration space for

a given temperature T and configuration x (a brief demonstration is provided in Appendix A) :

$$P_O(x) = \frac{\exp\left(\frac{-E(x)}{k_B T} + \ln(O(x))\right)}{Z_O(T)}. \quad (3)$$

This probability $P_O(x)$, targeted by PULSE, is a way to reconstruct $\langle O(T) \rangle$. Since $P_O(x)$ contains the logarithm of the property $O(x)$, this property must be strictly positive for each sample. Therefore, given that the observable can take various forms, it is necessary to ensure positivity of $O(x)$ in order for Eq. 3 to hold. We use a suited function built in such a way we can use it to sample a wide range of values of the observable despite the logarithm shape. Examples of this procedure are provided in the following sections.

2.2. Learning process

In this section, the goal is to learn $P_O(x)$ for each T . Since the space in which x lies is too large for a systematic exploration, we use an approach that involves constructing and using another distribution $P(y)$ that can be easily sampled from in order to recover $P_O(x)$. The auxiliary variable y acts as a compressed lower-dimensional representation of x ; its dimensionality is thus significantly smaller than that of x . To link these two distributions, we define a probability distribution $R(x|y)$. Since this distribution is arbitrary, its form must be optimised so that sampling x from it reproduces the target distribution $P_O(x)$.

To link $R(x|y)$ to $P_O(x)$, we then use Bayes' theorem with another conditional distribution $Q(y|x)$ that allows for inverse sampling :

$$P_O(x)Q(y|x) = P(y)R(x|y). \quad (4)$$

We then transform the ideal scenario of Eq. (4) into an optimisation problem, in which distributions R and Q (given in Appendix B, Eqs. B1-B3) are parameterised so that samples x drawn from $P(y)$ follow the target distribution $P_O(x)$. To do so, we use a classic tool to measure the difference between two distributions, *i.e.*, the Kullback-Leibler (KL) divergence [32] defined as follows :

$$\begin{aligned} D_{KL} [P(y)R(x|y) \parallel P_O(x)Q(y|x)] \\ &= \mathbb{E}_{y \sim P, x \sim R} \ln \left[\frac{P(y)R(x|y)}{P_O(x)Q(y|x)} \right] \\ &= -\mathbb{E}_{y \sim P, x \sim R} \ln \left[\frac{P_O(x)Q(y|x)}{P(y)R(x|y)} \right]. \end{aligned} \quad (5)$$

Since the KL divergence is always non-negative, we can write :

$$0 \leq -\mathbb{E}_{y \sim P, x \sim R} \ln \left[\frac{P_O(x)Q(y|x)}{P(y)R(x|y)} \right]. \quad (6)$$

and finally :

$$\ln Z_O \geq \mathbb{E}_{y \sim P, x \sim R} \ln \left[\frac{\exp\left(\frac{-E(x)}{k_B T} + \ln(F(O(x)))\right) Q(y|x)}{P(y)R(x|y)} \right]. \quad (7)$$

Hence, by maximizing the right-hand side of Eq. (7), we ensure that our model provides a lower bound of the partition function Z_O . In practice, our goal is to saturate this inequality and provide a reliable estimate of the partition function. Learning thus involves solving this optimization problem, based on which it is possible to build an ML architecture that is suitable for solving this type of problem. The parameters of the joint distributions R and Q are set via two neural networks (a decoder and an encoder, respectively) that, as learning converges, will enable the ideal equality of (4) to be approximated. Figure 1 shows the inverse-VAE architecture of our learning model : the networks encode and decode the information at the edges of the architecture in the latent space y . In each iteration, the model samples y from $P(y)$ and then samples configurations of the system x from $R(x|y)$. Since x is discrete, the Gumbel softmax trick [33] is applied to generate the samples from this continuous distribution. After calculations of energies and observable properties, results are given back to reconstruct a new latent space y' from $Q(y|x)$.

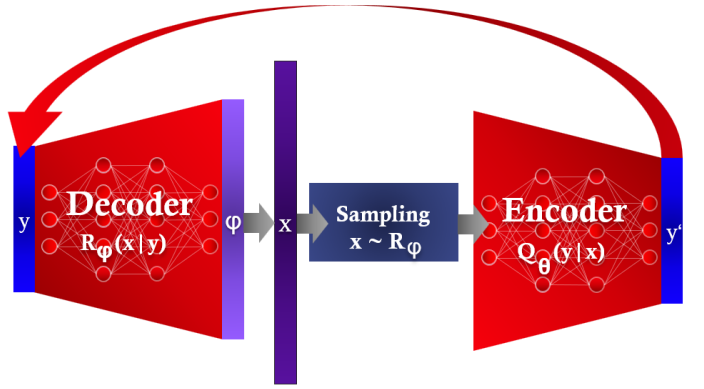


FIGURE 1 – Schematic view of the PULSE inverse VAE architecture.

All PULSE networks use the same architecture shown in Fig. 1, where the encoder and the decoder have the same architecture : three layers with a single hidden layer containing 2048 nodes, with SELU activation functions. Learning proceeds using the Adam optimizer [34] and a learning rate of 10^{-4} . The temperature parameter of the Gumbel softmax function [33] is set to $\tau = 1/10$.

3. Ising model

In this section, we introduce the Ising model and the properties chosen to assess our method. The objective is

twofold : first, to review the equations that govern this system, which will form the mathematical framework for our analysis; second, to establish an analogy between this simplified physical model and the systems targeted by PULSE. In this context, the Ising model serves as a well-understood version of a disordered two-component system that allows us to conduct an initial assessment of our method applied to the prediction of global thermodynamic properties. It should be mentioned that the 2D Ising system routinely serves as a benchmark for several developments in machine learning methods [24, 25, 26, 27, 28, 29], which have proved their effectiveness when applied to this system. It consists of a square lattice of size $N = L \times L$, where each site is occupied by a spin. These spins S_i can either be 'up' or 'down', i.e., $S_i = \pm 1 \forall i \in \{1, \dots, N\}$.

Interactions between these spins are described according to the following expression for the total energy E of the system, where i, j denotes nearest-neighbor interaction only :

$$E = -J \sum_{i,j} S_i S_j - H \sum_{i=1}^N S_i . \quad (8)$$

We consider the case with no external magnetic field ($H = 0$). The exchange energy J , controlling the interaction strength, is set to $J = 1$, which corresponds to the ferromagnetic case. We define the magnetization as the sum of the spins over the system :

$$M = \sum_{i=1}^N S_i . \quad (9)$$

In this configuration, the Ising system has two regimes that depend on temperature. At high temperature, the system is disordered, with no preferred spin orientation. At low temperature, spins are aligned either up or down, since there is no external magnetic field, with a phase transition occurring at the Curie temperature $T_C = 2/\ln(1 + \sqrt{2}) \approx 2.2693K$.

Our central interest in the study of this model lies in the analysis of the physical quantities of interest such as :

- The susceptibility χ :

$$\chi = \frac{\partial M}{\partial H} = N\beta(\langle M^2 \rangle - \langle M \rangle^2) . \quad (10)$$

- The specific heat at constant volume C_V :

$$C_V = \frac{\partial E}{\partial T} = N\beta^2(\langle E^2 \rangle - \langle E \rangle^2) . \quad (11)$$

with $\beta = \frac{1}{k_B T}$ and $k_B = 1$ for convenience.

For the latter property, we can directly relate this formulation for a 2D Ising system to the one that can be used for the heat capacity at constant volume in real physical compounds [35] :

$$C_V = \frac{1}{k_B T^2} (\langle U^2 \rangle - \langle U \rangle^2) . \quad (12)$$

where U represents the internal energy of the thermodynamic system. Indeed, this property is formulated as a combination of observable average properties of a chemically disordered system, so it can be sampled and estimated in the same way as the properties mentioned above in the Ising model framework.

We can write the thermodynamic averages of these quantities as ratios between different partition functions. For instance, for a given temperature T , let x be a given spin configuration. The average of the total magnetic moment is :

$$\langle M(T) \rangle = \frac{\sum_{x \in X} M_x(T) \exp(-\beta E_x(T))}{\sum_{x \in X} \exp(-\beta E_x(T))} . \quad (13)$$

We thus define two partition functions as follows :

$$Z(T) = \sum_{x \in X} \exp(-\beta E_x(T)) . \quad (14)$$

$$Z_M(T) = \sum_{x \in X} M_x(T) \exp(-\beta E_x(T)) . \quad (15)$$

so that :

$$\langle M(T) \rangle = \frac{Z_M(T)}{Z(T)} . \quad (16)$$

However, $\langle M \rangle$ cannot be calculated as such with PULSE because this quantity can be either positive or negative, while PULSE must learn on strictly positive values. Thus, in this work, we decide to target $\langle |M| \rangle$ instead of $\langle M \rangle$, which transforms χ into a distinct magnetic susceptibility χ' . This susceptibility χ' is still a quantity commonly studied in the Ising system [36, 37, 38]. We thus have :

$$Z_{|M|}(T) = \sum_{x \in X} \exp(-\beta E_x(T) + \ln |M_x(T)|) . \quad (17)$$

$$Z_{M^2}(T) = \sum_{x \in X} \exp(-\beta E_x(T) + \ln M_x^2(T)) . \quad (18)$$

To determine the susceptibility χ' , we rewrite equation (10) as :

$$\chi'(T) = N\beta \left(\frac{Z_{M^2}(T)}{Z(T)} - \left(\frac{Z_{|M|}(T)}{Z(T)} \right)^2 \right) . \quad (19)$$

The same development can be made for the specific heat at constant volume written as follows :

$$C_V(T) = N\beta^2 \left(\frac{Z_{E^2}(T)}{Z(T)} - \left(\frac{Z_E(T)}{Z(T)} \right)^2 \right) . \quad (20)$$

The associated partition functions are then :

$$Z_E(T) = \sum_{x \in X} \exp(-\beta E_x(T) + \ln[-E_x(T)]) . \quad (21)$$

$$Z_{E^2}(T) = \sum_{x \in X} \exp(-\beta E_x(T) + \ln[E_x^2(T)]) . \quad (22)$$

In Eq. (21), we sample $-E$ instead of E to calculate the associated partition function in Eq. (21). To deal with cases where the energy is positive – which are extreme cases, given that the average energy of this system is negative – we seek to exclude them from the training process by treating them as a near-zero ($< 10^{-8}$) observable. This choice is physically justified because very high-energy configurations do not contribute to the partition function especially in the low-temperature regime, where these high-energy values have low probability. As our sampling aims to calculate the partition function, the error made in excluding high-energy configurations should remain negligible.

4. Results

In this section, we assess the robustness of our method using several use cases and benchmarks. The first part examines the reliability of our model in estimating the aforementioned Ising properties. The second part demonstrates its scalability with respect to system size. Finally, we compare our method to specific Monte Carlo algorithms to evaluate the relative performance of our method.

As shown in Fig. 1, the PULSE model trains two networks, an encoder and a decoder, for each of the partition functions and for each temperature needed to reconstruct the thermodynamic data mentioned in Sec. 3 : Z , $Z_{|M|}$, Z_{M^2} , Z_E , and Z_{E^2} . Exact values are obtained by "brute-force" computations where all possible spin configurations are accounted for.

4.1. Benchmark on Ising properties

In this subsection, we use PULSE to estimate the specific magnetic susceptibility χ' of the Ising system. Results are normalised by the total number of spins N in the system. We apply this study to a 4×4 Ising lattice, which has 65 536 different configurations.

First, we estimate the partition functions necessary to build the target property as defined in Eq. (19). In Fig. 2, we show the PULSE estimate of the canonical partition function of the system (Eq. (14)), in good agreement with the exact solution (Eq. (14)), in good agreement with the exact solution, confirming the results already achieved in a previous work [18] where the inverse VAE concept was introduced and applied to the 2D Ising partition function. Here, PULSE reaches a remarkable accuracy, with an error below 1% compared to the exact value, using between 200 and 2 500 samples per temperature.

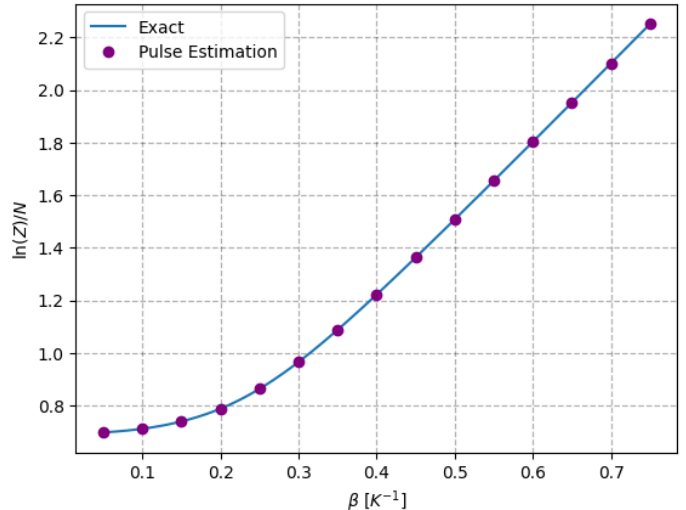


FIGURE 2 – Canonical partition function of the 4×4 Ising system, with the exact value (obtained by including all possible spin configurations in the calculation) shown as a blue curve and the PULSE estimation as purple dots. The convergence criterion is set to a 1% error relative to the exact value.

Figure 3 represents the PULSE estimation of $Z_{|M|}$, *i.e.*, the partition function associated with the absolute value of the magnetization (Eq. (17)). Similarly to the previous quantity, PULSE reaches an error below 1% compared to the exact value, using between 200 and 2 500 samples per temperature, depending on the target temperature. This shows that PULSE consistently achieves an outstanding accuracy on the partition function associated with specific properties, using a relatively low and stable amount of configurations.

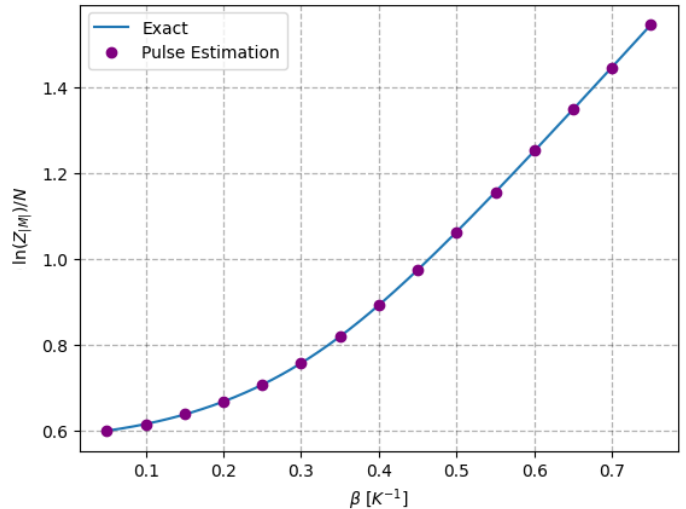


FIGURE 3 – Partition function of the absolute value of magnetization for the 4×4 Ising system, with the exact value (obtained by including all possible spin configurations in the calculation) shown as a blue curve and the PULSE estimation as purple dots. The convergence criterion is set to a 1% error relative to the exact value.

This high precision in our estimations allows us to properly predict properties that depend on those partition functions, as shown in Fig. 4 for the properties needed to obtain the modified susceptibility χ' . These plots show respectively estimations of average modified magnetization, squared magnetization, and modified susceptibility as presented in Eqs. (16) through (19). Purple symbols correspond to quantities obtained by combining the different estimations of PULSE at each temperature.

For properties that rely on the combination of two partition functions, *i.e.*, equal to the ratio between the partition function of the observable property and the canonical partition function, as in Eq. (16), the PULSE evaluation is in excellent agreement with the exact solution (see Figure 4 (a) for the average modified magnetization, and Figure 4 (b) for the average squared magnetization). On the other hand, properties that are combination of more than two partition functions, as in Eq. (19), present slight deviations at low temperature. This is the case for the modified magnetic susceptibility (see Figure 4 (c)).

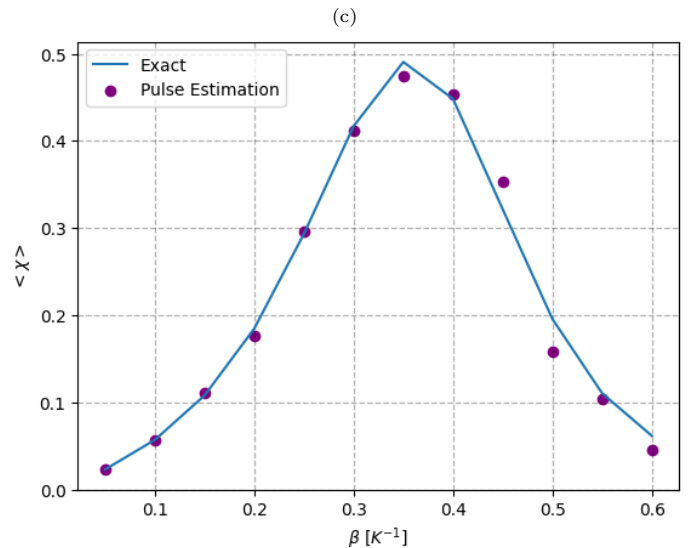
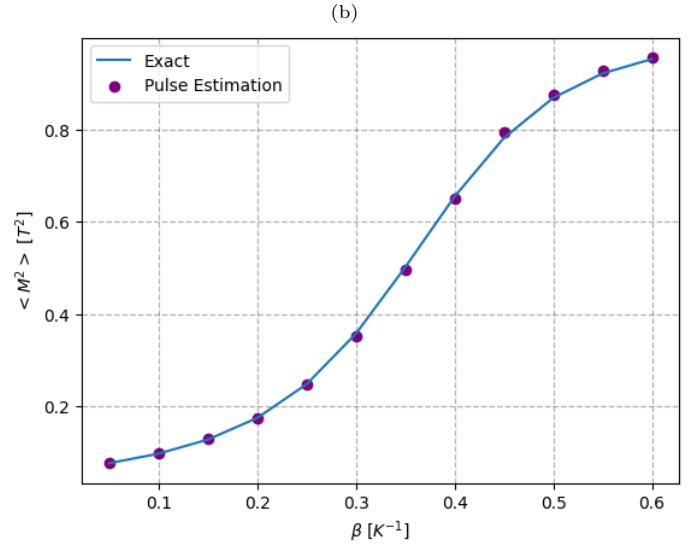
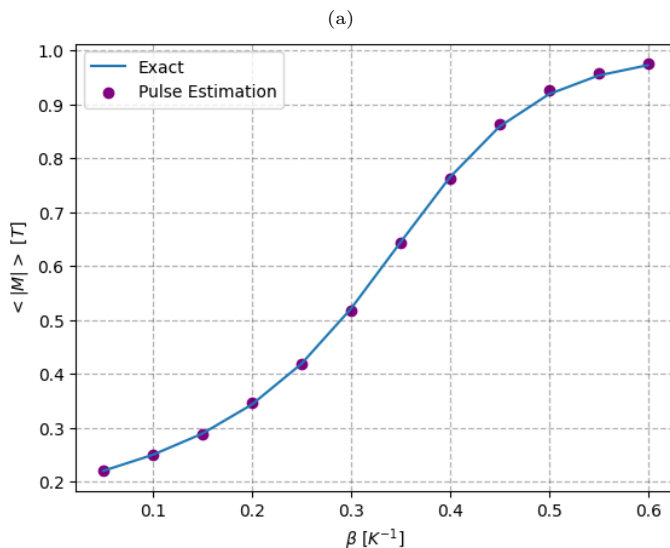


FIGURE 4 – Average values of (a) normalized magnetization, (b) squared magnetization, and (c) modified susceptibility obtained as recombinations of partition functions sampled by PULSE. Purple dots are recombinations of partition functions according to equations (14), (17), and (18). The blue curve marks the exact value (obtained by including all possible spin configurations in the calculation).

This likely arises because at low temperature (and therefore high β), the Ising system is restricted to two significant states that correspond to the configurations where all spins are aligned either 'up' or all 'down'. PULSE has difficulties finding these states and performs better at high temperatures, when more configurations contribute significantly to the partition function. In addition, the errors in the various estimates accumulate in the reconstruction of the property. Nevertheless, it is important to note that the results are displayed in Fig. 4 on a linear scale, which accentuates errors that are otherwise negligible on the logarithmic scale on which our model operates. For instance, for $\beta = 0.5 \text{ K}^{-1}$, the error

is 15% on a linear scale, but only 2.7% on a logarithmic scale. The performance of the method is therefore satisfactory : accurate predictions of the target properties can be obtained with few samples and thus low computational cost.

4.2. Scalability

In this section, we investigate the robustness of our sampling method with respect to system size to assess its stability and scalability. In Fig. 5, we compare three different evaluations of the partition function associated with energy Z_E , as in Eq. (21), to the exact values for Ising systems of size varying from 3×3 to 5×5 . For these calculations, we consider the learning converged when the estimated error is below 1%.

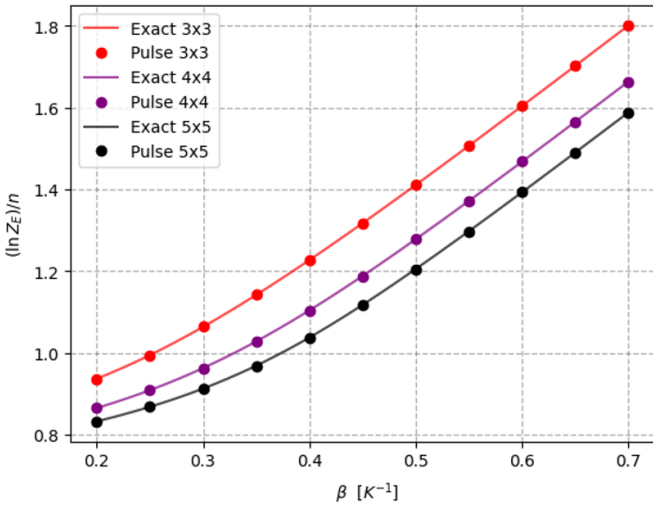


FIGURE 5 – Energy-related partition functions of 2D Ising systems sampled by PULSE for different system sizes : 3×3 (512 configurations), 4×4 (65 536 configurations) and 5×5 (33 554 432 configurations), compared to exact values (obtained by including all possible spin configurations in the calculation).

For any system size, the amount of configurations needed in the sampling procedure does not exceed 2000 samples per temperature, and we find that the larger the system, the fewer samples are actually needed. For a 3×3 Ising system, the algorithm requires on average between 1500 and 2000 samples, whereas for a system of size 5×5 , it requires around 500 to 1000 samples per temperature.

This result provides initial evidence of the good scalability of our method : system size has a small impact on the amount of configurations needed to obtain a satisfying accuracy, and the algorithm seemingly converges better as the system has a larger number of spins. Furthermore, this result also allows us to confirm the validity of our method for sampling Z_E , despite the neglect of states with positive energy discussed in Section 3.

The fact that, for the 3×3 Ising system, our method requires more samples than available states in the configuration space ($2^{(3 \times 3)} = 512$) can be explained by the fact that

our method is not designed to handle such small systems, where exhaustive exploration is feasible. This architecture is intended to infer properties of very large configuration spaces, as we will show below.

Because of the exponentially increasing number of possible configurations, it is difficult to compare with the exact solution at larger scales. From the 6×6 system onwards, there are several billion configurations to sample to calculate the exact solution (over 6.8×10^{10} samples for 6×6 and over 5.62×10^{14} samples for 7×7).

In Fig. 6, we demonstrate the scalability of our method by extending it to larger Ising system sizes (from 3×3 to 60×60). Each learning process is performed with 2000 samples using the same PULSE model architecture. The objective is to examine the trends in the curves produced by PULSE and assess if, despite the increase in system size, the expected behavior is recovered. Each curve is obtained from 10 independent models in order to average the estimations and provide error bars.

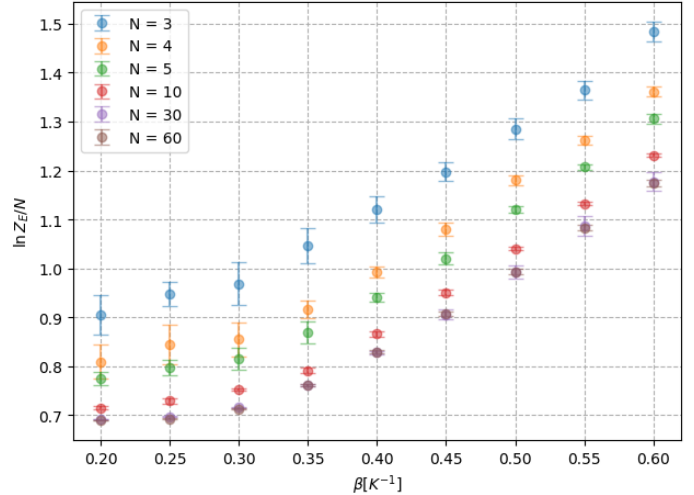


FIGURE 6 – Energy-related partition functions of 2D Ising systems estimated by PULSE for system sizes ranging from 3×3 to 60×60 .

We can see that the trend estimated in Fig. 5 is accurately reproduced : $\ln Z_E/N$ increases with increasing β and decreases. We also find that convergence improves as the number of spin increases : indeed, for all temperatures, we observe a reduction in error bars at large system sizes.

In light of these results, we conclude that PULSE is robust with respect to system size : without changing the size of the model, very few samples (relative to the size of the configuration space) are needed to achieve convergence. This is a clear advantage for studying real, more complex physical systems.

4.3. Comparison with Monte-Carlo

In this last section, we compare our results with another typically method used to estimate mean properties in disorde-

red compounds : Monte Carlo. For sampling the Ising lattice system, we use two Monte Carlo algorithms specifically designed for this type of systems : Wolff [20] and Wang-Landau [39].

Instead of randomly flipping individual spins, as in conventional Monte Carlo methods, Wolff’s algorithm flips entire clusters of spins. As a result, correlated spins are flipped simultaneously, allowing for a more efficient exploration of the configuration space. However, this method is not designed to estimate partition functions, but rather observable properties of the system. It thus needs to be adapted to enable comparisons with the PULSE method.

To this end, let Z be the canonical partition function of the Ising system and $|X|$ the number of configurations of this system. We can write :

$$\begin{aligned} \frac{1}{Z} &= \sum_{x \in X} \frac{1}{|X|Z} = \sum_{x \in X} \frac{\exp(\beta E(x) - \beta E(x))}{|X|Z} \\ &= \frac{1}{|X|} \sum_{x \in X} \exp(\beta E(x)) p(x), \end{aligned} \quad (23)$$

where :

$$p(x) = \frac{\exp(-\beta E(x))}{Z}. \quad (24)$$

So by taking m samples of the system, obtained using the Monte Carlo scheme, we can estimate Z in the following way :

$$\frac{1}{Z} = \frac{1}{|X|} \mathbb{E}_{x \sim p(x)}[\exp(\beta E(x))] \approx \frac{1}{|X|m} \sum_{j=1}^m \exp(\beta E(x)), \quad (25)$$

with :

$$x \sim p(x). \quad (26)$$

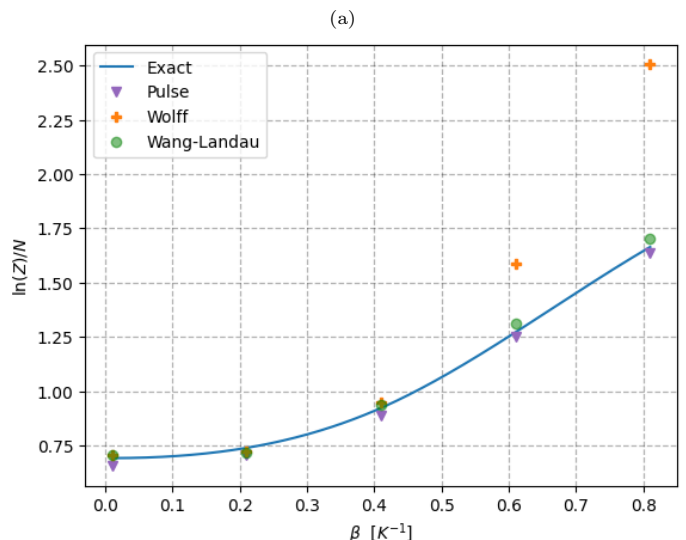
The second Monte Carlo method we consider is the the Wang-Landau method, a standard choice for estimating partition functions. It is a Monte Carlo algorithm that, instead of sampling configurations according to Boltzmann’s law, performs a uniform random walk in energy in order to estimate the density of states and ultimately the canonical partition function of the system. Further details on this method can be found elsewhere[39]. It should be noted that, since this method must uniformly explore the energy space, it is difficult to ensure convergence for large system sizes. This technique is therefore introduced for comparison purposes, but is not well suited to the thermodynamic property prediction applications considered for PULSE.

We now compare partition function sampling using these methods. In Fig. 7 (a), we present results from PULSE, Wolff, and Wang-Landau for the estimation of a canonical partition function, together with the number of samples needed Fig. 7

(b). For this comparison, we set the convergence criterion to a 1% error relative to the exact value. If this precision is not reached after 40 000 samples, the algorithm is stopped.

For this partition function, Wolff’s algorithm fails to sample the system accurately beyond the phase transition ($\beta \approx 0.4 \text{ K}^{-1}$). Since convergence is limited to 40 000 samples by choice, Wolff sampling stops with an error of 29.1% and 83.9% for $\beta = 0.6 \text{ K}^{-1}$ and $\beta = 0.7 \text{ K}^{-1}$, respectively. So, in this context, we see that PULSE provides a significantly better estimate of the canonical partition function of the Ising system, while requiring fewer samples than Wolff, which is designed to estimate thermodynamic properties. This is expected, as Wolff’s algorithm does not require explicit evaluation of the partition function to estimate mean properties. Instead, averages are obtained directly from sampled configurations, regardless of whether or not they are representative of the partition function.

Concerning the Wang-Landau algorithm, designed instead to estimate partition functions, results are comparable to those of PULSE, but more configurations are required to converge at high temperatures. Furthermore, results deviate slightly more from the exact value at low temperatures.



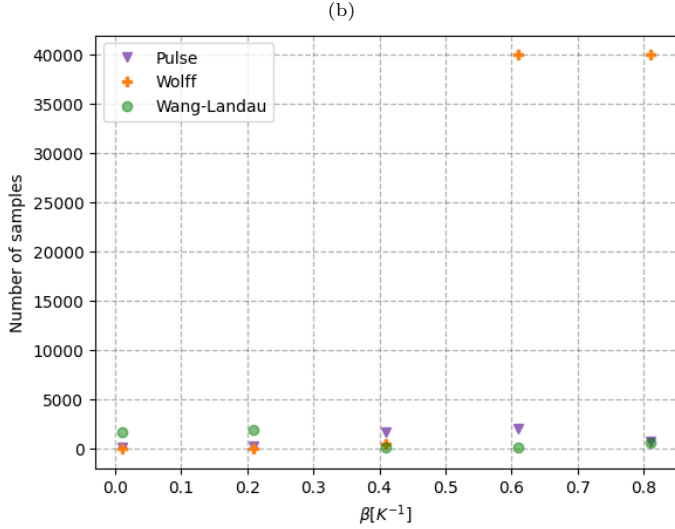


FIGURE 7 – Comparison of sampling methods for the canonical partition function of the 2D Ising system. (a) Canonical partition function of a 4×4 Ising system estimated by different sampling method. (b) Number of samples required for each sampling at each temperature.

A more relevant comparison is to compare the performance of PULSE and both Monte Carlo methods in estimating thermodynamic properties such as the average energy and the associated heat capacity, as defined in Eq. (20).

For this comparison, we perform 10 independent evaluations per property, using 2 000 samples for each temperature and method. This allows us to account for statistical uncertainties inherent to our stochastic approach. Reported values thus correspond to the average of these 10 estimates, with uncertainties obtained by calculating the standard deviation. The uncertainties on the combinations of PULSE estimates are obtained by error propagation.

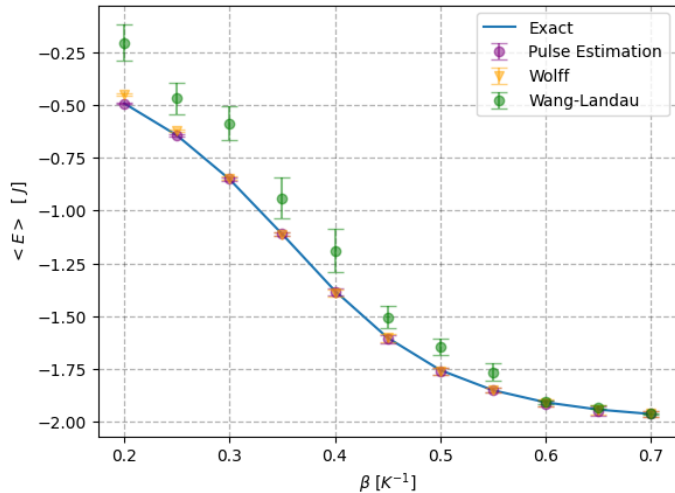


FIGURE 8 – Comparison of sampling methods for the average energy of the 2D Ising system using PULSE, Wolff, and Wang-Landau algorithms.

Figure 8 shows the results of the three methods for the mean energy of the Ising system. All methods produce values close to the exact results, except for Wang-Landau at low β (we observe for instance error exceeding 50% at $\beta = 0.2 \text{ K}^{-1}$). Figure 9 shows the corresponding errors relative to the exact solution, along with uncertainty estimates. It should be noted that each method yields better results in different temperature regimes. Wolff’s algorithm performs better at low temperatures ($\beta \gtrsim 0.4 \text{ K}^{-1}$), because, as mentioned above, PULSE has difficulties in finding representative states in this temperature range. In contrast, Wolff’s algorithm easily finds these states where the spins are all aligned thanks to its algorithm allowing updating aligned clusters all at ones. In the other temperature regime ($\beta \lesssim 0.4 \text{ K}^{-1}$), characterized by disordered states, the opposite behaviour is observed : PULSE achieves a very high accuracy, whereas Wolff’s error increases with temperature and with the number of significant Ising states in the energy calculation. Finally, Wang-Landau performs well at very low temperatures ($\beta \gtrsim 0.6 \text{ K}^{-1}$), where it finds the representative states of the partition function easily, but very poorly at higher temperature. This behaviour is expected, as this method is not designed to estimate mean properties in the same way as standard Monte Carlo methods, and it thus needs significantly more samples to converge in the high-temperature regime. Indeed, since it explores configurations regardless of their energy, it requires more configurations to converge when there are more energy levels that are significant for the partition function.

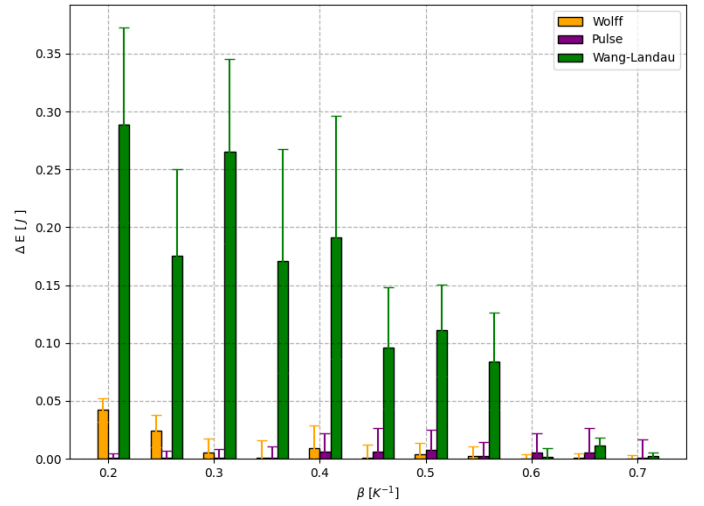


FIGURE 9 – Comparison of errors in the sampling of the average energy using PULSE, Wolff, and Wang-Landau algorithms.

Finally, these energy estimates are used to reconstruct the target property, i.e., the specific heat at constant volume (cf. Eq. 20). We show in Fig. 10 the results of all methods, and in Fig. 11 the corresponding errors.

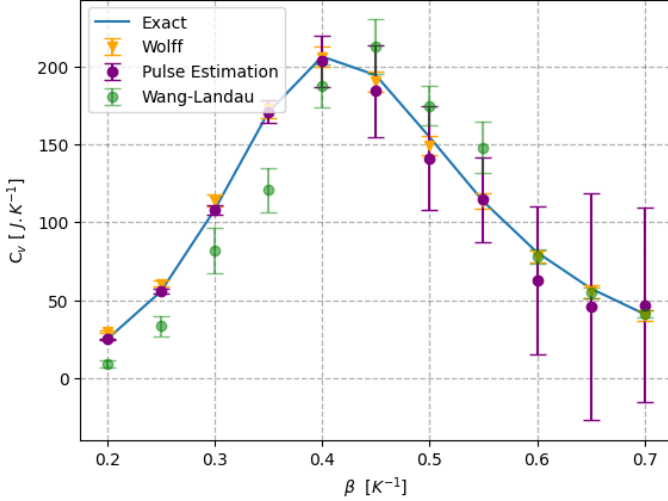


FIGURE 10 – Comparison of sampling of mean specific heat by PULSE, Wolff and Wang-Landau with error bars.

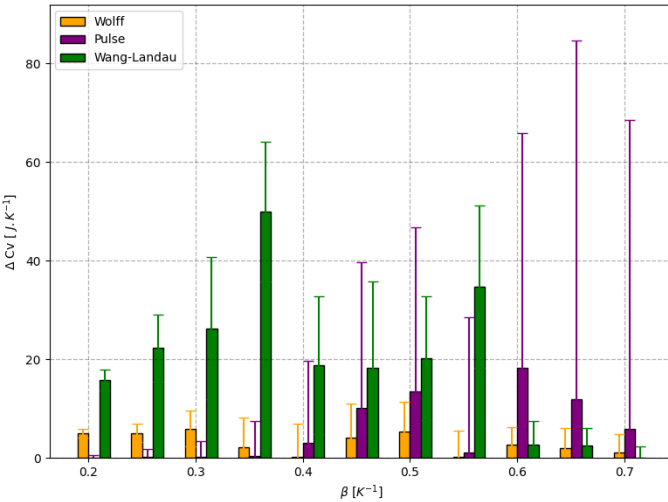


FIGURE 11 – Comparison of errors in the sampling of the average specific heat by PULSE, Wolff, and Wang-Landau algorithms.

For this property, the previously observed trends are confirmed. Figure 10 and 11 clearly show that each sampling method seems more suited to a specific temperature range. As the PULSE method struggles to find the few most significant states at low temperature, the deviations from the exact solution are slightly larger, and the error bars more significant in this temperature range. On the other hand, for small β ($< 0.4 \text{ K}^{-1}$), PULSE is in excellent agreement with the exact value, better than Wolff in this temperature range. Also, we find again that Wang-Landau performs well only at very low temperatures ($\beta \gtrsim 0.6 \text{ K}^{-1}$).

The behaviour of our PULSE algorithm is therefore promising for future applications addressing the thermodynamic properties of disordered materials. With a relatively low

number of samples, PULSE provides excellent estimates of the target property, outperforming the capabilities of the benchmark Monte Carlo methods in the high-temperature regime, while keeping the error in the low-temperature regime at acceptable levels. Most notably, it is usually the high-temperature range, where PULSE performs best, that is the most interesting for many applications, including nuclear ones. For this reason, conditions where very few configurations only are representative of the entire system (effectively tending towards a more ordered compound) is not a typical situation that this algorithm has been designed to treat. It is also important to note that reconstructing properties using multiple partition functions, as done for instance for the specific heat, inevitably impacts the accuracy of the PULSE estimations due to error propagation, whereas Wolff does not suffer from this issue as it directly estimates said target property. Finally, contrary to most sampling methods currently available, a key advantage of PULSE is that it provides both a way to sample the partition function of the system and an estimate of it, which is particularly valuable for physical exploitation.

Finally, we can add a perspective for improving our model in light of these results. Our model operates with few assumptions about the configuration space to be explored, and appears to have difficulties sampling very specific cases, *i.e.*, finding configurations with all spins aligned at low temperature. One idea for the future development of PULSE would be to add assumptions about the physical environment to be studied, if we have prior knowledge of it. For instance, in our previous work [17] the PULSE loss function was tweaked to take into account the nominal Pu concentration in the generated atomic configurations.

5. Conclusions

In this work, we extended the recently introduced PULSE method [17] to make it suitable for computing thermodynamic properties of chemically disordered materials. In this regard, we have developed a novel general theoretical framework that allows PULSE to estimate observable properties through atomic-scale calculations and the optimized sampling of the configuration space of disordered materials.

We tested this method on the 2D Ising system, which is mathematically very similar to the target systems. The effectiveness of this approach has been proven in several ways. Firstly, it estimates the properties of the system with good accuracy from a small number of samples and therefore at a low computational cost. Secondly, it is stable and scalable with respect to system size, as the number of samples needed for convergence does not depend on the latter. Without changing the model’s architecture, we are able to obtain estimates of the target properties with considerably few samples compared to the size of the configuration spaces studied. Finally, the comparison with Monte Carlo sampling methods

such as Wolff and Wang-Landau demonstrates its ability to provide accurate estimates of a wide range of properties, with a particularly effective sampling of disordered states at high temperatures, which is interesting for future applications to disordered materials. Low-temperature estimates are slightly less accurate due to accumulation of errors on the various partition functions combined to compute the target property. Nevertheless, the low-temperature behavior of the Ising system, where few highly ordered states dominate, represents an extreme case that is unlikely to occur in real disordered materials. Future developments could include incorporating prior knowledge about the physical environment to improve the model performance in handling very specific cases

Considering the excellent results on the Ising system, the PULSE method fully achieves its objective of providing an efficient sampling and evaluation of the properties of disordered systems, as we had already begun in our previous study [17]. This paves the way to the application of the method to the thermodynamic properties of real disordered compounds, such as mixed-oxide nuclear fuels or high-entropy alloys; with applications that could make use of our generative tool, for example to generate training datasets for ML interatomic potentials.

In conclusion, PULSE represents a significant advance in addressing the properties of chemically disordered compounds, providing a computationally efficient way to sample their partition function while estimating target properties of interest for the technological application of these materials. In this respect, its upcoming application to thermodynamic properties is expected to substantially enhance the characterization of these compounds.

Acknowledgments

This work was performed using HPC resources from GENCI TGCC Joliot-Curie under allocation 2025-A0180906008. It contributes to the CEA RTA/RCOMB project and received funding from the CEA CFR program. The authors thank R. Santet for fruitful discussions about the mathematical framework.

Data availability statement

The data that support the findings of this study are available upon reasonable request.

Author declarations

Conflict of interest

The authors have no conflicts to disclose.

Appendix

A/ Probability definition

It should be noted that the formulation of the partition function for an observable O is as follows :

$$Z_O(T) = \sum_{x \in X} O(x) \exp\left(\frac{-E(x)}{k_B T}\right)$$

By factorising the exponential, we can then write : (27)

$$= \sum_{x \in X} \exp\left(\frac{-E(x)}{k_B T} + \ln(O(x))\right) .$$

Eq. 3 is therefore obtained following this formulation to define the probability of finding a state x with the value O :

$$P_O(x) = \frac{\exp\left(\frac{-E(x)}{k_B T} + \ln(O(x))\right)}{Z_O(T)} . \quad (28)$$

B/ Definition of joint distributions

Following previous works [17, 18] function $R_\phi(x|y)$ is defined as a product distribution, with ϕ being a neural network :

$$R_\phi(x|y) = \prod_i \frac{e^{I(x^{(i)}) \phi^{(i)}(y)}}{e^{\phi^{(i)}(y)} + e^{-\phi^{(i)}(y)}} , \quad (29)$$

with I an indicator function defined as follows for the Ising system :

$$I(x^{(i)}) = \begin{cases} 1 & \text{if } x^{(i)} \text{ represents a spin up,} \\ -1 & \text{if } x^{(i)} \text{ represents a spin down.} \end{cases} \quad (30)$$

$Q_\theta(y|x)$ follows the same logic but reversed, with θ being a neural network :

$$Q_\theta(y|x) = \prod_i \frac{e^{y^{(i)} \theta^{(i)}(x)}}{e^{\theta^{(i)}(x)} + e^{-\theta^{(i)}(x)}} . \quad (31)$$

Notes and references

- [1] D. Shin, R. Arróyave, Z.-K. Liu, A. Van de Walle, Thermodynamic properties of binary hcp solution phases from special quasirandom structures, *Physical Review B—Condensed Matter and Materials Physics* 74 (2006) 024204.
- [2] J.-F. Vigier, P. M. Martin, L. Martel, D. Prieur, A. C. Scheinost, J. Somers, Structural investigation of (u0.7pu0.3) o2-x mixed oxides, *Inorganic chemistry* 54 (2015) 5358–5365.

- [3] S. Wei, F. He, C. C. Tasan, Metastability in high-entropy alloys : A review, *Journal of Materials Research* 33 (2018) 2924–2937.
- [4] M.-H. Tsai, J.-W. Yeh, High-entropy alloys : a critical review, *Materials Research Letters* 2 (2014) 107–123.
- [5] A. Ostovari Moghaddam, A. Cabot, E. A. Trofimov, Does the pathway for development of next generation nuclear materials straightly go through high-entropy materials?, *International Journal of Refractory Metals and Hard Materials* 97 (2021) 105504. doi :<https://doi.org/10.1016/j.ijrmhm.2021.105504>.
- [6] M. C. Gao, D. E. Alman, Searching for next single-phase high-entropy alloy compositions, *Entropy* 15 (2013) 4504–4519. doi :[10.3390/e15104504](https://doi.org/10.3390/e15104504).
- [7] E. J. Pickering, A. W. Carruthers, P. J. Barron, S. C. Middleburgh, D. E. Armstrong, A. S. Gandy, High-entropy alloys for advanced nuclear applications, *Entropy* 23 (2021) 98.
- [8] S. Zinkle, 16 - advanced irradiation-resistant materials for generation iv nuclear reactors, in : P. Yvon (Ed.), *Structural Materials for Generation IV Nuclear Reactors*, Woodhead Publishing, 2017, pp. 569–594. doi :<https://doi.org/10.1016/B978-0-08-100906-2.00016-1>.
- [9] Y. Zhang, Y. J. Zhou, J. P. Lin, G. L. Chen, P. K. Liaw, Solid-solution phase formation rules for multi-component alloys, *Advanced engineering materials* 10 (2008) 534–538.
- [10] M. C. Gao, C. Niu, C. Jiang, D. L. Irving, *Applications of Special Quasi-random Structures to High-Entropy Alloys*, Springer International Publishing, Cham, 2016, pp. 333–368.
- [11] D. H. Case, J. E. Campbell, P. J. Bygrave, G. M. Day, Convergence properties of crystal structure prediction by quasi-random sampling, *Journal of chemical theory and computation* 12 (2016) 910–924.
- [12] S.-H. Wei, L. Ferreira, J. E. Bernard, A. Zunger, Electronic properties of random alloys : Special quasirandom structures, *Physical Review B* 42 (1990) 9622.
- [13] C. Takoukam-Takoundjou, E. Bourasseau, V. Lachet, Study of thermodynamic properties of u1-y-puyo2 mox fuel using classical molecular monte carlo simulations, *Journal of Nuclear Materials* 534 (2020) 152125. doi :<https://doi.org/10.1016/j.jnucmat.2020.152125>.
- [14] Y. LeCun, Y. Bengio, G. Hinton, Deep learning, *nature* 521 (2015) 436–444.
- [15] X. Liu, J. Zhang, Z. Pei, Machine learning for high-entropy alloys : Progress, challenges and opportunities, *Progress in Materials Science* 131 (2023) 101018.
- [16] F. Tan, L. Li, J. Li, B. Liu, P. K. Liaw, Q. Fang, Multiscale modelling of irradiation damage behavior in high entropy alloys, *Advanced Powder Materials* 2 (2023) 100114. doi :<https://doi.org/10.1016/j.apmate.2023.100114>.
- [17] M. J. Karcz, L. Messina, E. Kawasaki, E. Bourasseau, Targeting the partition function of chemically disordered materials with a generative approach based on inverse variational autoencoders, *arXiv preprint arXiv :2408.14928* (2024).
- [18] G. T. Cantwell, Approximate sampling and estimation of partition functions using neural networks, *arXiv preprint arXiv :2209.10423* (2022).
- [19] D. Landau, Finite-size behavior of the ising square lattice, *Physical Review B* 13 (1976) 2997.
- [20] U. Wolff, Collective monte carlo updating for spin systems, *Physical Review Letters* 62 (1989) 361.
- [21] L. Onsager, Crystal statistics. i. a two-dimensional model with an order-disorder transition, *Physical review* 65 (1944) 117.
- [22] Y. Zhang, Ising spin configurations with the deep learning method, *Journal of Physics Communications* 5 (2021) 015006.
- [23] G. Torlai, R. G. Melko, Learning thermodynamics with boltzmann machines, *Physical Review B* 94 (2016) 165134.
- [24] F. D’Angelo, L. Böttcher, Learning the ising model with generative neural networks, *Physical Review Research* 2 (2020) 023266.
- [25] C. Alexandrou, A. Athenodorou, C. Chrysostomou, S. Paul, The critical temperature of the 2d-ising model through deep learning autoencoders, *The European Physical Journal B* 93 (2020) 226.
- [26] S. J. Wetzel, Unsupervised learning of phase transitions : From principal component analysis to variational autoencoders, *Physical Review E* 96 (2017) 022140.
- [27] W. Hu, R. R. Singh, R. T. Scalettar, Discovering phases, phase transitions, and crossovers through unsupervised machine learning : A critical examination, *Physical Review E* 95 (2017) 062122.
- [28] N. Walker, K.-M. Tam, M. Jarrell, Deep learning on the 2-dimensional ising model to extract the crossover region with a variational autoencoder, *Scientific reports* 10 (2020) 13047.

- [29] R. C. Alamino, Explaining the machine learning solution of the ising model, arXiv preprint arXiv :2402.11701 (2024).
- [30] D. Yevick, Variational autoencoder analysis of ising model statistical distributions and phase transitions, The European Physical Journal B 95 (2022) 56.
- [31] D. P. Kingma, M. Welling, Auto-encoding variational bayes, arXiv preprint arXiv :1312.6114 (2013).
- [32] S. Kullback, R. A. Leibler, On information and sufficiency, The annals of mathematical statistics 22 (1951) 79–86.
- [33] E. Jang, S. Gu, B. Poole, Categorical reparameterization with gumbel-softmax, arXiv preprint arXiv :1611.01144 (2016).
- [34] D. P. Kingma, J. Ba, Adam : A method for stochastic optimization, arXiv preprint arXiv :1412.6980 (2014).
- [35] M. Lagache, P. Ungerer, A. Boutin, A. Fuchs, Prediction of thermodynamic derivative properties of fluids by monte carlo simulation, Physical Chemistry Chemical Physics 3 (2001) 4333–4339.
- [36] A. Murtazaev, M. Ramazanov, M. Badiev, Critical properties of the two-dimensional ising model on a square lattice with competing interactions, Physica B : Condensed Matter 476 (2015) 1–5.
- [37] E. Albano, A. De Virgiliis, M. Müller, K. Binder, Corner wetting in the two-dimensional ising model : Monte carlo results, Journal of Physics : Condensed Matter 15 (2003) 333–345.
- [38] L. N. Shchur, O. A. Vasilyev, Critical amplitude ratio of the susceptibility in the random-site two-dimensional ising model, Physical Review E 65 (2001) 016107.
- [39] F. Wang, D. Landau, Determining the density of states for classical statistical models : A random walk algorithm to produce a flat histogram, Physical Review E 64 (2001) 056101.